XL CILAMCE
IBERO-LATIN AMERICAN CONGRESS ON COMPUTATIONAL METHODS IN ENGINEERING
NOVEMBER 11-14, 2019
Praiamar Natal Hotel & Convention
Natal, RN-BRAZIL

FINITE ELEMENT MODELLING OF PLANE FRAME SUBJECTED TO RANDOM WIND EXCITATION WITH DYNAMIC ELASTOPLASTIC BEHAVIOR

Hsu Yang Shang
hsu.shang@pucpr.br
Igor Alexandre Deitos
igor.deitos@gmail.com

Pontifícia Universidade Católica do Paraná, Polytechnic School, Graduate Program in Mechanical Engineering. Rua Imaculada Conceição, 1155, Prado Velho, CEP 80215-901, Curitiba, Paraná, Brazil.

Abstract. This work presents a finite element approach of dynamic elastoplastic analysis in plane frame subjected to random excitation caused by wind action. The wind random velocity is modelled mathematically by using Power Spectra Density Method in combination with Shinozuka's model, with commonly employed wind spectra, such as von Kármán, Davenport, Kaimal and Harris. From these spectra, the dynamic wind loading is determined from the sum of the mean and floating wind velocities. Thus, it is possible to obtain the wind loading vector that is applied in the structure dynamic governing equation. The governing equation is formulated by Euler-Bernoulli beam theory, and it is discretized by using a conventional Lagrange – Hermite element. The time stepping process is carry out by HHT algorithm, and the material nonlinearity is modelled by von Mises isotropic hardening model. Finally, several applications are presented, where different wind spectra are employed to determine mechanical parameters of structure responses, such as stress, strain, displacement, among the other. The error norm L_2 of displacement is determined for different finite element discretization refine, which aims to analyze the effects of space discretization in this type of analysis. Also, the relative differences are determined with the purpose to compare the different mechanical behavior of structure when subjected to different wind spectra.

Keywords: Finite element modelling, Power spectral density, random wind loadings, Elastoplastic structure behavior, Error in norm L_2 of displacement.

1 Introduction

Nowadays, steel structures are used in almost all construction sectors, such as industrial sheds, buildings, telecommunications towers, chimneys, among others. Its usage has increased significantly due to its versatility, ease of manufacture, high reliability and its well-defined mechanical properties. Due to these reasons, the project design of steel structure has gained more complexity in the recent decades. The growth of urban centers, characterized by scanty regions of horizontal space, leads to the necessity to have buildings even taller. Consequently, these are more susceptible to problems of wind excitation, which is characterized as random behavior. Furthermore, this behavior provides loading conditions that could generate resonant vibration and elastoplastic deformation in the structure, leading it to possible collapse [34]. Therefore, the prediction of structure yielding conditions and collapse conditions subjected to a random excitation plays an important role during the development phase of project design, since the wind action has been one of the accidents causes in tall buildings around the world. However, the analysis of structural random behavior is complex and analytical solution is not always possible in the situation that involves multiple degrees of freedom. Therefore, due to the recent advances in computational mechanics and proposal of new numerical methods, the modelling of steel frame has become more accurate during the project design phase. Such model makes the numerical approach more assertive with less computational processing time.

This work aims to present a numerical modelling of plane frame subjected to random excitation considering that the structure suffers dynamic elastoplastic deformation. For wind action modeling, the Power Spectral Density Method is adopted, and several wind spectra are employed for the numerical approach. Moreover, the method proposed by Shinozuka and Jan (1972) is adopted to calculate the wind velocity. Besides, the Finite Element Method is adopted for structure discretization and a Lagrange – Hermite linear element with three nodes is employed to discretize the governing equation, which is formulated by Euler – Bernoulli beam theory. Furthermore, for structure elastoplastic behavior, the von Mises isotropic hardening model is employed. Several applications are carried out to show the competitiveness of the proposed numerical modelling. Moreover, the error in norm L2 of displacement is determined. In the following, a brief literature review is presented.

Experiments carried out in wind tunnels have shown a relationship between the distribution of fluctuating pressures of the floating wind in the atmospheric boundary layer with the incoming conditions [13]. And this relationship is expressed by the Reynolds number [21][11][35]. To obtain more reliable responses of the dynamic wind loading, researchers usually use wind tunnel aeroelastic models [16][38]. Furthermore, the combination of numerical methods and probabilistic methods through the computational tools has enabled the solution of problems that involves the random loading of wind in complex structures [5][19].

Dynamic analyses are commonly suggested in tall and slender structures subjected to vibrations induced by wind loads [23][28], such as in the Taipei 101 Tower skyscraper, where there are natural events such as earthquakes and hurricanes [25]. To analyze the inelastic responses of wind-excited in tall buildings, [12] perform a comparative analysis for the differences between elastic and inelastic responses through two statistical linearization approaches. The first elastoplastic analysis of plane frames has begun in the early 60's, shortly after the birth of digital computers, with the numerical model positioning the plastic hinges below the maximum point of beams [24]. This consideration serves as a reference for many researches that introduce nonlinear behavior into plane frame structures [23]. Other methodologies of nonlinear analysis have been developed with the Euller-Bernoulli beam theory, where effects due to shear and torsion were neglected, or Timshenko beam theory. Another important aspect in the study of dynamic elastoplastic behavior of structures is the yielding criterion adopted in the analysis. Thus, the von Mises criterion is widely used in the researches [31]. An important advantage of the steel structures is its ductility, which becomes a main characteristic in the studies of elastoplastic analysis due to the fact that it provides more mechanical strength to the structure, in comparison with other material [18][6]. Three-dimensional steel plane frames are employed in the numerical approach where the material and geometrical nonlinearities are developed

through the controlled displacement technique or generalized displacements technique [22][30].

The study of elastodynamics phenomenon has begun in 1972. The main issue in this area of study is the estimation of spatial and temporal errors that are inherent in the employed numerical approaches. Thus, the method proposed by Goudreau and Taylor (1972) for the capture of wave propagation uses beam finite element [14]. A few years later, for time increment algorithm, other researchers developed several methods, modified from Newmark method [25], such as HHT [17], which aims to insert an adjustable parameter to control the numerical dissipation. Furthermore, the Newmark linear acceleration methods do not guarantee the numerical stability in the analysis of structures with nonlinear behavior [25][1]. Therefore, some algorithms based on the momentum conservation and energy dissipation were developed to guarantee the second order precision and stability in nonlinear problem [10][1][29][7]. Recently, developments of enriched finite element approach, such as the Generalized Finite Element Method are strongly investigated in the dynamic elastoplastic analyses to verify the enriched elements quality and efficiency [32][33].

2 Modelling of Wind Excitation

Wind excitation plays an important role in the dynamic analysis of slender steel frames. Further, the wind actions present random characteristics and make its prediction difficult to be done by deterministic treatment [36]. Therefore, wind power density spectra (Kim *et al.*, 2001) are tools widely employed for the determination of wind loadings. The wind loading is calculated based on its velocity [26]:

$$V(z,t) = \bar{V}(z) + v(z,t) \tag{1}$$

where $V(z,t)$ is the wind velocity as a function of time and height, $\bar{V}(z)$ is the average velocity, a parameter determined by NBR 6123 (1988), and $v(z,t)$ is the floating velocity.

Over the years, many researchers have devoted efforts to develop several mathematical expressions that represent the wind random excitation, based on measurements and experimental results. The most common used spectra are those proposed by Kaimal, Davenport, Harris, Lumley and Panowski and von Kármán [35], as shown in Table 1, where f is the frequency, in Hz; $S_v(f)$ is the spectral density of the longitudinal component of turbulence in the frequency f; $x(f)$ is the dimensionless frequency; u_* is the friction velocity; V_{10} is the average wind velocity at 10 m above ground level, in m/s. For spectra that vary with frequency and height, the V_z is equal to the average wind velocity in m/s, above ground level z, which is the height of load application in m; the von Kármán constant, k, is 0,4 [35] and the roughness length, z_0, is 0,07 m.

Table 1 – Wind power spectral density functions.

	DAVENPORT	HARRIS	LUMLEY & PANOWSKY	KAIMAL	VON KÁRMÁN
PSD	$\frac{fS_v(f)}{{u_*}^2} = 4\frac{x^2}{(1+x^2)^{\frac{4}{3}}}$	$\frac{fS_v(f)}{{u_*}^2} = 4\frac{x}{(2+x^2)^{\frac{5}{6}}}$	$\frac{fS_v(f)}{{u_*}^2} = 4\frac{x}{1+x^{\frac{5}{3}}}$	$\frac{fS_v(f,z)}{{u_*}^2} = \frac{200x}{(1+50x)^{\frac{5}{3}}}$	$\frac{fS_v(f,z)}{{u_*}^2} = \frac{24x_u}{(1+70.7x_u{}^2)^{\frac{5}{6}}}$
VARIABLES	$x(f) = \frac{1200f}{V_{10}}$	$x(f) = \frac{1800f}{V_{10}}$	$x(f) = \frac{900f}{V_{10}}$	$x(f,z) = \frac{fz}{V_z}$ $u_* = \frac{k\bar{V}_z}{\ln\left(\frac{z}{z_0}\right)}$	$x_u = L_{ux}x_{(f,z)}$ $L_{ux} = 300\left(\frac{z}{350}\right)^{\frac{1}{k}}$ $\frac{1}{k} = 0.437 + 0.153\log z_0$

In Figure 1, the abscissa axis presents the number of waves in cycles per meter and the ordinate axis presents the power spectral density normalized by the variance. In this case, the total energy of the system is represented proportionally by the area delimited under the curve of the frequencies. The power density spectra depicted in Figure 1 are divided into two main groups: velocity that dependents the height and the frequency, and velocity that is independent of the height. The power spectra with wind velocity independent of the structure height, are Davenport, Harris and Lumley and Panowsky. Besides, the spectra of Kaimal and von Kármán have the velocity dependents the height and frequency.

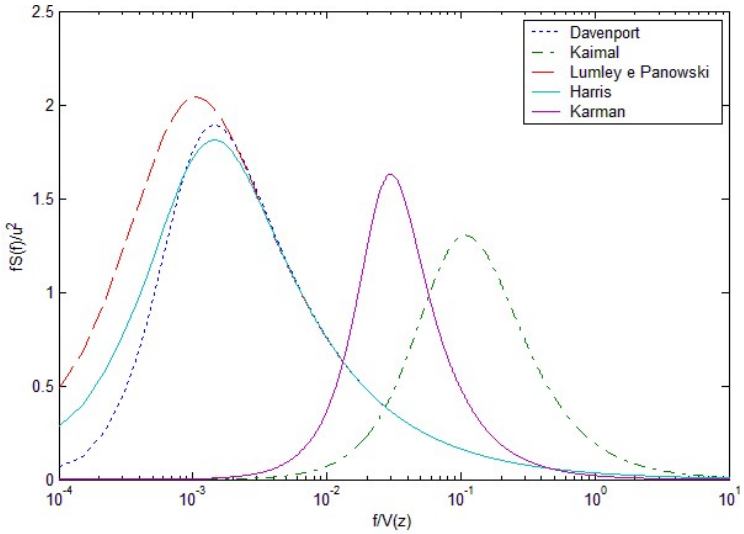

Figure 1 – Wind power spectral density curves.

Studies concerning the determination of wind velocity randomness over time are developed using the digital simulation technique based on multivariate random processes [34], which serve as an essential tool for large numbers of problems in structural engineering, such as numerical analysis of dynamic nonlinear response in structures subjected to random excitations; analysis of linear structures under random excitations in time and frequency domain; numerical approach of wave propagation in a random medium and solution of eigenvalue problems in structures with randomly nonhomogeneous materials. As one of commonly used method, the essential aspect of Shinozuka and Jan's approach (1972) states that the random process can be simulated by a series of trigonometric functions with random frequency, or wave number.

The present work adopts the method proposed by Shinozuka and Jan (1972), where the floating part of the wind velocity is inserted into a stationary random process. This part is determined by the superposition of harmonic waves, as represented by Equation 2:

$$v(t) = \sum_{i=1}^{N} \sqrt{2S^{v}(f_i)\Delta f}\,\cos(2\pi f_i t + \theta_i) \tag{2}$$

where N is the number of divisions in the power spectral density; $S^{v}(f_i)$ is the power density spectrum of the longitudinal turbulence component of the frequency f; Δf is the increment of frequency, in Hz; f_i is the variation of the frequency range, in Hz; t is the time, in second and θ_i is the random phase angle, between 0 and 2π. Thus, the equation of the dynamic pressure represented in the Brazilian Association of Technical Standards (1988) is rewritten as follows:

$$q(z,t) = 0{,}613(\bar{V}_z + v(z,t))^2 \tag{3}$$

where $q(z,t)$ is the dynamic pressure of the wind as a function of height and time, in N/m²; $\bar{V}_z$ is the average wind velocity, in m/s and $v(z,t)$ is the floating part of wind velocity, in m/s. After

determining the dynamic pressure of the wind as a function of time and height, it is necessary to determine the force acting on the structure:

$$F(z,t) = C_{ai} q(z,t) A_i \tag{4}$$

where $F(z,t)$ is the load acting on the structure as a function of height and time, in N; C_{ai} is the coefficient of drag [3] and A_i is the area of influence of the load, in m². After obtaining the equation (4), it is used in the structure governing equilibrium equation to be presented in following section.

3 Structure Governing Equations

This section briefly presents the formulation of the structural vibration phenomenon considered in this work and its finite element discretization. Consider an isotropic, homogeneous solid with volume V, and Euler – Bernoulli beam theory, the governing equation of motion of such body is:

$$\rho A \frac{\partial^2 u_1}{\partial t^2} - E(x,t) A \frac{\partial^2 u_1}{\partial x^2} = f_{u_1}(x,t) \tag{5a}$$

$$\rho A \frac{\partial^2 u_2}{\partial t^2} + \frac{\partial^2}{\partial x^2}\left(E(x,t) I \frac{\partial^2 u_2}{\partial x^2}\right) = f_{u_2}(x,t) \tag{5b}$$

where ρ is the mass density, u_1 and u_2 is the displacement in axial and transversal direction, respectively, A and I is area and moment of inertia, respectively, $E(x,t)$ is the elastoplastic modulus, $f_{u_1}(x,t)$ and $f_{u_2}(x,t)$ is the force in axial and transversal direction, respectively.

The Total Lagrangian Formulation is used to describe the elastoplastic dynamic behavior of the solid. Consider the infinitesimal strain, small displacement and elastoplastic behavior, the weak form of governing equation is derived by the principle of virtual displacements:

$$\int_V \left[\delta u^T \rho \ddot{u} + S_{ij} \delta \varepsilon_{ij}\right] dV = R(t) \tag{6}$$

where S_{ij} is the second Piola-Kirchoff stress tensor, ε_{ij} is the Green-Lagrange strain tensor, δu is the virtual displacement, and $R(t)$ is the time dependent external virtual work. The Green-Lagrange strain tensor can be evaluated by Eq. (7), which includes the nonlinear terms.

$$\varepsilon_{ij} = \frac{1}{2}\left(u_{i,j} + u_{j,i} + u_{k,i} u_{k,j}\right) \tag{7}$$

The finite element discretization is done here by using Euler-Bernoulli beam element with three nodes, depicted in Figure 2. The element field displacements are evaluated according to Eq. (8).

$$\boldsymbol{u} = \boldsymbol{N u_e} \tag{8}$$

where $\boldsymbol{u_e}$ is the vector of nodal values in element coordinates, and $\boldsymbol{N}$ is the matrix of beam shape function, constituted by Lagrange – Hermite polynomials. Introducing Eq. (7) and Eq. (8) into Eq. (6), and neglecting damping effect, the finite element equilibrium equations are derived:

$$\begin{aligned} \sum \int_{L_E} \boldsymbol{\delta u_e}^T \boldsymbol{N}^T \boldsymbol{\rho A N \ddot{u}_e} \boldsymbol{dx} + \sum \int_{L_E} \boldsymbol{\delta u_e}^T \boldsymbol{B^L}^T \boldsymbol{D^{EP}} \boldsymbol{B^L u_e dx} + \\ + \sum \int_{L_E} \boldsymbol{\delta u_e}^T \left(\boldsymbol{B_1^{NL}}^T \boldsymbol{F} \boldsymbol{B_1^{NL}} + \boldsymbol{B^L}^T \boldsymbol{M} \boldsymbol{B_2^{NL}}\right) \boldsymbol{u_e dx} = \\ = \sum \boldsymbol{\delta u_e}^T \boldsymbol{P_{ext}^e} - \sum \int_{L_E} \boldsymbol{\delta u_e}^T \boldsymbol{B^L}^T \boldsymbol{P\, dx} \end{aligned} \tag{9}$$

Where $\boldsymbol{B^L}$ is the linear strain-displacement matrix, $\boldsymbol{B_1^{NL}}$ and $\boldsymbol{B_2^{NL}}$ are nonlinear strain-displacement matrices, ρ is the density, A is the cross-section area, and $\boldsymbol{D^{EP}}$ is the constitutive matrix, which is updated according to the von Mises isotropic hardening model, and $\boldsymbol{P}$ is comprised by equivalent forces $\boldsymbol{F}$ and equivalent moments $\boldsymbol{M}$. Further, $\boldsymbol{u_e}$and $\boldsymbol{\ddot{u}_e}$ are the element nodal displacements and accelerations, respectively, $\boldsymbol{N}$ are the shape functions, and $\boldsymbol{P_{ext}^e}$ are the external forces, produced by wind random excitation.

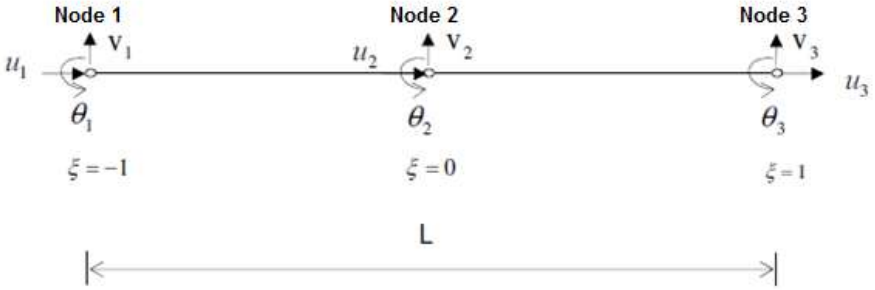

Figure 2 – Three-nodes element.

The equation (9) can also be represented in the following element coordinate equation:

$$\boldsymbol{M^e} = \int_{L_E} \boldsymbol{N^T \rho A N dx} \tag{10a}$$

$$\boldsymbol{K_{EP}^e} = \int_{L_E} \boldsymbol{B^{L^T} D^P B^L dx} \tag{10b}$$

$$\boldsymbol{K_G^e} = \int_{L_E} \left(\boldsymbol{B_1^{NL^T} F B_1^{NL}} + \boldsymbol{B_2^{NL^T} M B_2^{NL}} \right) \boldsymbol{dx} \tag{10c}$$

$$\boldsymbol{Q_P^e} = \int_{L_E} \boldsymbol{B^{L^T} P \, dx} \tag{10d}$$

where $\boldsymbol{M^e}$ is the element mass matrix, $\boldsymbol{K_{EP}^e}$ is the element elastoplastic stiffness matrix, which is updated according to stress level, $\boldsymbol{K_G^e}$ is the element geometric stiffness matrix, which is updated at each iteration due to equivalent force and moment, and, finally, $\boldsymbol{Q_P^e}$ is the residual force vector. After introducing Eq. (10a) through Eq. (10d) into Eq. (9), with proper coordinate transformation and element assembling, the finite element global equilibrium equations reduce to:

$$\boldsymbol{M\ddot{u} + Ku = f(t)} \tag{11}$$

The matrix of shape function $\boldsymbol{N}$ used in previous equation is defined by equation (12a). In addition, the linear and nonlinear strain – displacement matrices are defined by equations (12b) – (12d):

$$\boldsymbol{N} = \begin{bmatrix} N_1 & 0 & 0 & N_4 & 0 & 0 & N_7 & 0 & 0 \\ 0 & N_2 & N_3 & 0 & N_5 & N_6 & 0 & N_8 & N_9 \end{bmatrix} \tag{12a}$$

$$\boldsymbol{B^L} = \begin{bmatrix} N_1' & 0 & 0 & N_4' & 0 & 0 & N_7' & 0 & 0 \\ 0 & N_2'' & N_3'' & 0 & N_5'' & N_6'' & 0 & N_8'' & N_9'' \end{bmatrix} \tag{12b}$$

$$\boldsymbol{B_1^{NL}} = \begin{bmatrix} N_1' & 0 & 0 & N_4' & 0 & 0 & N_7' & 0 & 0 \\ 0 & N_2' & N_3' & 0 & N_5' & N_6' & 0 & N_8' & N_9' \end{bmatrix} \tag{12c}$$

$$\boldsymbol{B_2^{NL}} = \begin{bmatrix} 0 & N_2'' & N_3'' & 0 & N_5'' & N_6'' & 0 & N_8'' & N_9'' \\ N_1' & 0 & 0 & N_4' & 0 & 0 & N_7' & 0 & 0 \end{bmatrix} \tag{12d}$$

The constitutive matrix $\boldsymbol{D^{EP}}$ is defined by the stress-strain relationship of material. The von Mises model is adopted for isotropic hardening. By using indicial notation for Cartesian axes, the incremental stress is given by [2]:

$$d\sigma_{ij} = D^{ep}_{ijkl} d\varepsilon_{kl} \tag{13}$$

The equation (13) is written incrementally for constitutive law, where the incremental strain components $d\varepsilon_{ij}$ are defined as a sum of linear strain and nonlinear strain from expansion of Taylor series. In equation (13), D^{ep}_{ijkl} is a tangential tensor defined by suitable state variables, such as constitutive tensor and effective stress, among others. Additionally, in this work, appropriate directions are also considered for D^{ep}_{ijkl} in unidimensional problems. Within the context of isotropic work hardening theory, the tangent constitutive tensor is defined as:

$$D^{ep}_{ijkl} = D_{ijkl} - (1/\gamma) D_{ijmn} a_{mn} a_{op} D_{opkl} \tag{14}$$

Where

$$D_{ijkl} = 2\mu\nu/(1-2\nu)\,\delta_{ij}\delta_{kl} + \mu\left(\delta_{ik}\delta_{ji} + \delta_{il}\delta_{jk}\right) \tag{15}$$

$$a_{kl} = \partial\bar{\sigma}/\partial\sigma_{kl} \tag{16a}$$

$$\gamma = a_{ij} D_{ijkl} a_{kl} + H \tag{16b}$$

$$H = \partial\sigma_o/\partial\bar{\varepsilon}^P \tag{16c}$$

In equation (16a) – (16c), $\bar{\sigma}$ and $\bar{\varepsilon}^P$ are the effective stress and plastic strain, respectively; σ_0 is the uniaxial yield stress; H is the plastic hardening modulus and μ and ν stand for the material shear modulus and the Poisson ratio, respectively. In case of von Mises isotropic strain-hardening material, the tensor of incremental elastoplastic material moduli takes the form $D^{ep}_{ijkl} = D_{ijkl} - \left(3\mu/\left(\sigma_0^2(1+H/3)\right)\right) s_{ij}s_{kl}$, where $s_{ij} = \sigma_{ij} - (1/3)\delta_{ij}\sigma_{kk}$ is the stress deviator; and for the case of a perfectly plastic material, $H = 0$. In case of elastic analyses, the Cauchy stresses can be defined by $\sigma_{ij} = D_{ijkl}\varepsilon_{kl}$, where D_{ijkl} is the elastic constitutive tensor.

For the initial stress formulation, it is convenient to define a fictitious "elastic" stress increment as follows:

$$d\sigma^e_{ij} = D_{ijkl} d\varepsilon_{kl} \tag{17}$$

And equation (13) can be rewritten as indicated below

$$d\sigma_{ij} = d\sigma^e_{ij} - d\sigma^P_{ij} \tag{18}$$

Where the initial stress increments are computed by

$$d\sigma^P_{ij} = (1/\gamma) D_{ijmn} a_{mn} a_{kl} d\sigma^e_{kl} \tag{19}$$

In present work, an a-posteriori error estimator is adopted in a simple form. The error in norm L_2 for displacement is calculated, as stated in expression (20). In addition, several refinement in spatial discretization is adopted in present work, therefore, the error is measured between different degree of refinement in the finite element discretization. This consideration is made due to limitation to found a literature results to be considered as a reference.

$$\|e\|_{L_2} = \left[\int_\Omega (u-\hat{u})^T (u-\hat{u}) d\Omega\right]^{1/2} \tag{20}$$

The flowchart, presented in Figure 3, shows the numerical solution procedure. The solution procedure begins with the input data for plane frame mechanical properties, follows by input data to evaluate the synthetic accelerogram by using power spectral density function. Then, the HHT algorithm is activated to calculate the nodal displacement vector, which is used to evaluate the strain,

then the von Mises stress is calculated. Then the von Mises criterion is initiated to verify if the plane frame is undergoing material hardening. If affirmative, the Newton- Raphson algorithm is initiated to update the new stress state of the material, and stiffness matrix is updated by changing the material modulus according to stress – strain relationship. Otherwise, the algorithm continues to verify the loading and unloading condition. The global convergence is verified in each point mesh of the plane frame. This work uses a point mesh constituted by seven point of numerical integration along the element. In every numerical integration point, the hardening condition is verified in the cross section. After this procedure, the residual force of pipe and foundation is calculated, and convergence condition is verified. This work adopts energy criterion to evaluate the convergence parameter with the tolerance value defined as $1x10^{-8}$. This loop continues until the convergence condition is fulfilled. Finally, the time step is incremented, and the procedure is restarted.

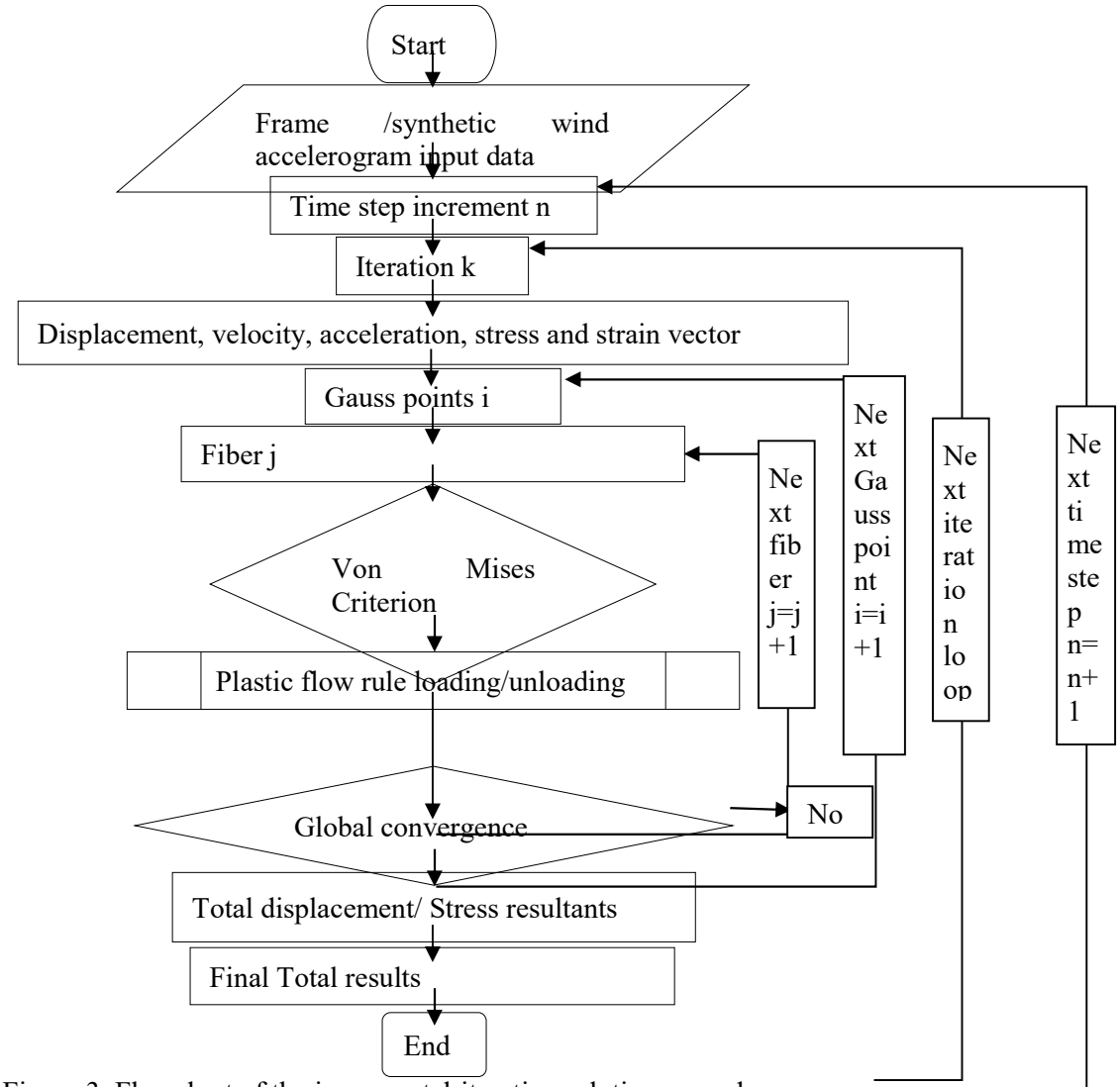

Figure 3. Flowchart of the incremental-iterative solution procedure.

4 Applications

This work adopts structural steel ASTM A36 [21] as material for the following analyses. The stress-strain relationship of this material is established by Ramberg-Osgood equation, as it is stated in equation (21):

$$\sigma = E\varepsilon\left[1 + \left(\frac{\varepsilon}{\varepsilon_0}\right)^n\right]^{\frac{-1}{n}} \tag{21}$$

Where the Young's modulus for steel, E, is 166.667 MPa; the yield stress, σ, is 250 MPa; the stress-strain parameter, n, is 1,798 and the initial strain, ε_0, is 0,0015 ($\varepsilon_0 = \sigma/E$). The material density, ρ, is 7830 kg/m³, and Poisson coefficient, v, is 0,3. Effect of damping is neglected.

In this work, the first application presents free vibration analysis. The second application presents the dynamic elastoplastic analyses of steel frame proposed by Orbison *et al*. (1982) and it is subjected to the wind loading modelled by spectra proposed by Kaimal [35]. The input data adopted for the following three applications are presented in Table 2. In addition, the table 3 presents the geometric properties of the structures. The HHT method [18] is adopted with α=1/3.

Table 2 - Data to calculate the wind loading, a roadmap for the examples.

Parameters		Unit	Origin
Height of point A $[z]$	9,144	m	Node coordinate
Exponential coefficient $[p]$	0,15	-	NBR-6123:1988
Roughness length $[z_0]$	0,07	m	NBR-6123:1988
Basic wind velocity $[V_0]$	45	m/s	NBR-6123:1988
Topographic factor $[S_1]$	1,0	-	NBR-6123:1988
Statistical factor $[S_3]$	1,0	-	NBR-6123:1988
Average velocity at 10 m $[V_{10}]$	31,05	m/s	-
Average velocity in Z quota $[V_z]$	Variable	m/s	-
Initial frequency $[f_0]$	0,010	H_z	Assumed
Final Frequency $[f_f]$	9,510	H_z	Assumed
Frequency range divisions $[N]$	100	-	Assumed
Frequency increment $[\Delta f]$	0,095	H_z	$(f_f\text{-}f_f)/100$
Initial time $[t_0]$	0,0	s	Assumed
Steps	250.000	-	Assumed
Time increment $[\Delta T]$	0,001	s	Assumed
Final time $[t_f]$	250,0	s	$(t_f$ x $\Delta T)$
Friction velocity $[u_*]$	Variable	m/s	-
PSD $[S_v(f,z)]$	Variable	-	-
Phase angle (0-2π) $[\theta_i]$	-	-	Random
Floating wind velocity $[V(z,t)]$	Variable	m/s	-
Dynamic pressure $[q(z,t)]$	Variable	N/m^2	-
Wind loading $[F(z,t)]$	Variable	N	-
Drag coefficient $[C_{ai}]$	1,50	-	Assumed
Width of influence area $[b]$	5,00	m	Assumed

Table 3 – Cross sectional properties of the structural elements.

Parameters		Unit
Horizontal beam length $[L]$	4,572	m
Horizontal beam cross-sectional area $[A_e]$	0,0047	m^2
Horizontal beam moment of inertia $[I_x = I_y]$	13,3x10^{-6}	m^4
Vertical beam length $[L]$	9,144	m
Vertical beam cross-sectional area $[A_e]$	0,0004	m^2
Vertical beam moment of inertia $[I_x = I_y]$	0,106x10^{-6}	m^4

1.1 Free vibration analysis of plane frame using FEM3

Table 4. First ten modes of natural frequency of FEM3.

	Ansys Beam 188	FEM3			
dof	2691	45	99	207	423
Mode					
1	31,3757	31,8035	31,8035	31,8035	31,8035
2	97,1883	98,4630	98,4627	98,4627	98,4627
3	160,4600	162,4355	162,4310	162,4310	162,4310
4	261,0663	265,0555	265,0715	265,0712	265,0712
5	295,7684	302,5289	302,5948	302,5943	302,5943
6	317,5145	326,1567	326,2795	326,2787	326,2787
7	545,7826	564,5898	564,2142	564,2065	564,2065
8	615,2684	621,8889	620,0581	620,0638	620,0638
9	632,0884	666,3821	669,4541	669,4304	669,4304
10	651,3778	684,2713	686,6102	686,5914	686,5913

1.2 Dynamic elastoplastic analysis of the modified Orbison plane steel frame

This example presents analyses of a plane frame with parameters adopted by Orbison *et al*. (1982), and it is shown schematically in the figure 4(b). The floating part of the velocity is determined by Kaimal power spectrum. The finite element mesh is consisted by refining **h**, where present 4 meshes. The purpose of this example is to validate the computational code, developed in present work, by making comparisons with well-known finite element code.

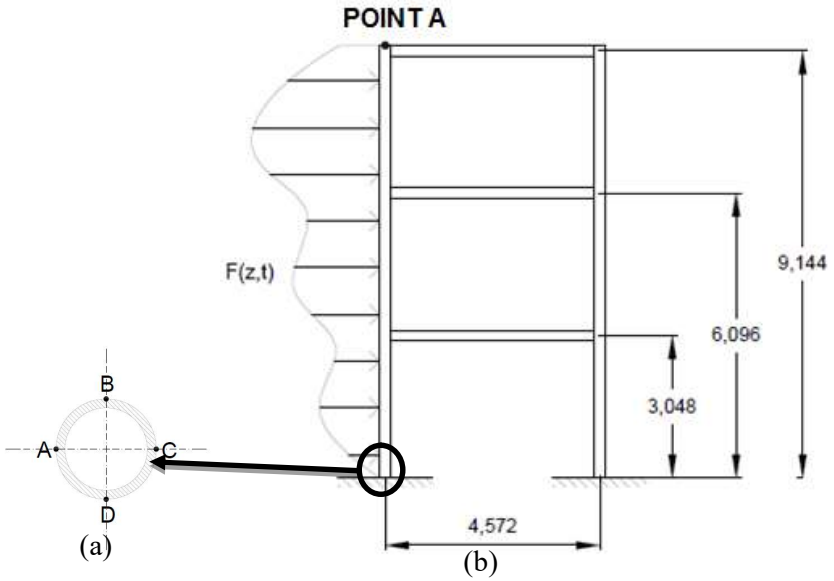

Figure 4 – a) Cross section; b) Plane steel frame analyzed with the action of random wind loading, unit (m).

For effects of visualization, the wind loading distribution along the height of the structure is depicted in t = 125 seconds, obtained with time increment $\Delta t = 10^{-3}$ s, as shown in Figure 5. Further, it is possible to observe the randomness in the behavior nature over the height.

For a better visualization of the behavior of the wind loading distribution over the time, Figure 6a shows the wind loading at point A from 100 to 101 s, and Figure 6b shows a zoom of this curve between the time interval of 100,1 and 100,2s. The Figures 7 show the displacement, velocity and acceleration profile in horizontal direction at the point A of the plane steel frame. The displacement shown in Figure 7a occurs during the structure yielding at 125s, with the magnitude approximately equal to 0,1 m. The velocity and acceleration profiles are also presented in Figure 7b and 7c, respectively. For better analysis of results, Figure 8a, Figure 9a and Figure 10a, show the results, over the time range covered by present example, which is 250 seconds. While Figures 8b, 9b and 10b show a zoom of the curves for the first 5 seconds. The randomness over the time is observed in all cases.

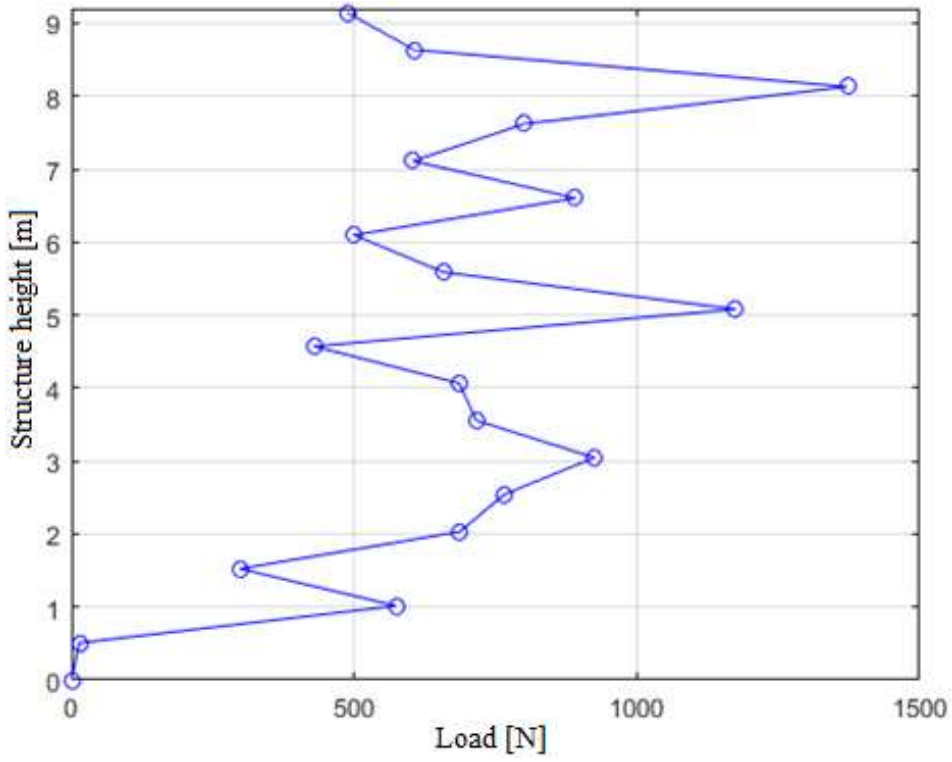

Figure 5 – Wind loading profile along the height of the structure at t = 125 s.

The von Mises stress is determined at vertical beam cross section's point A, as shown in Figure 4a. It may be observed in the Figure 11 that the material yielding initiates with strain $1{,}5x10^{-3}$ and stress 250 MPa, caused by compression, as presented by the material properties of ASTM A36. After this instance, the material hardening continues, until the moment of unloading. The process of loading and unloading repeats consecutively and material hardening does not occur again, due to the material hardening in the plane steel frame during first yielding process.

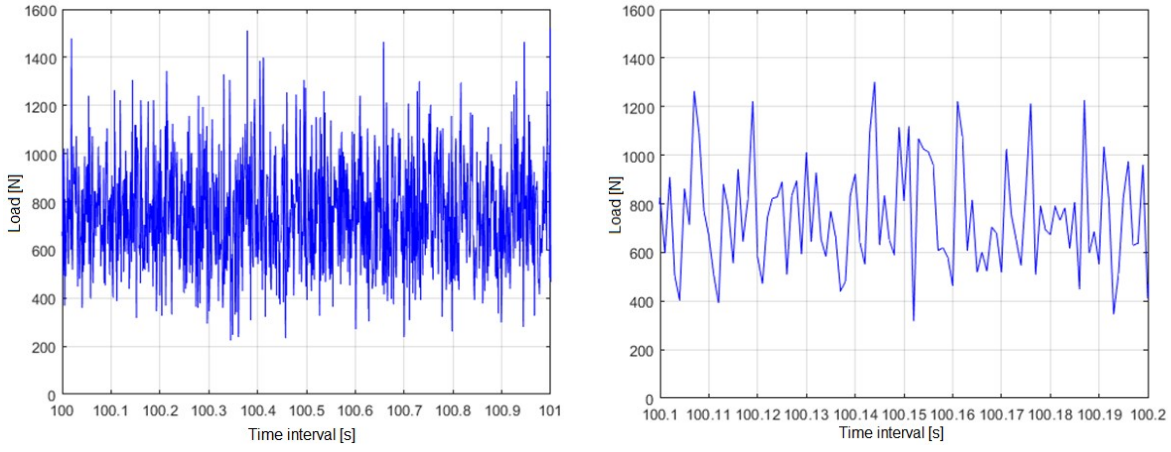

(a) (b)

Figure 6 –Behavior of the wind load curve at point A.

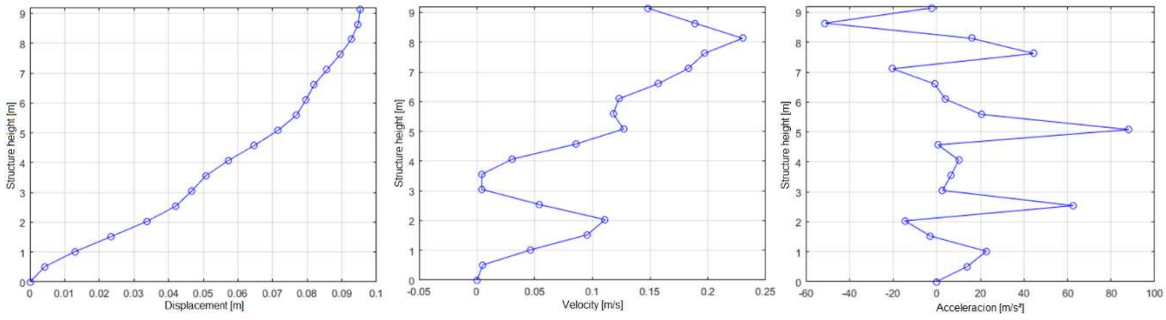

(a) (b) (c)

Figure 7 - Responses profile along the height of the structure at t = 125 s.

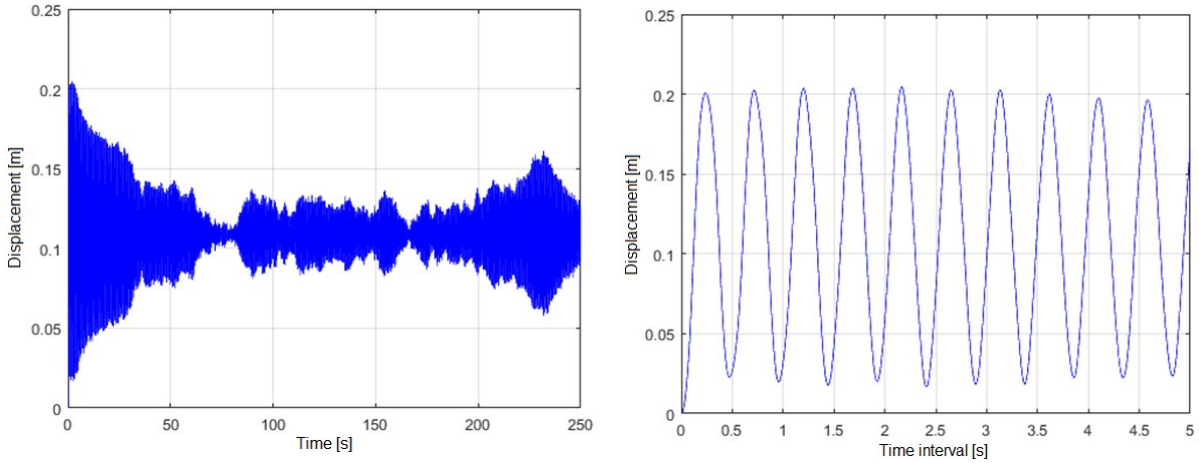

(a) (b)

Figure 8 – Displacement at point A at t = 250 s (a) and zoom in (b).

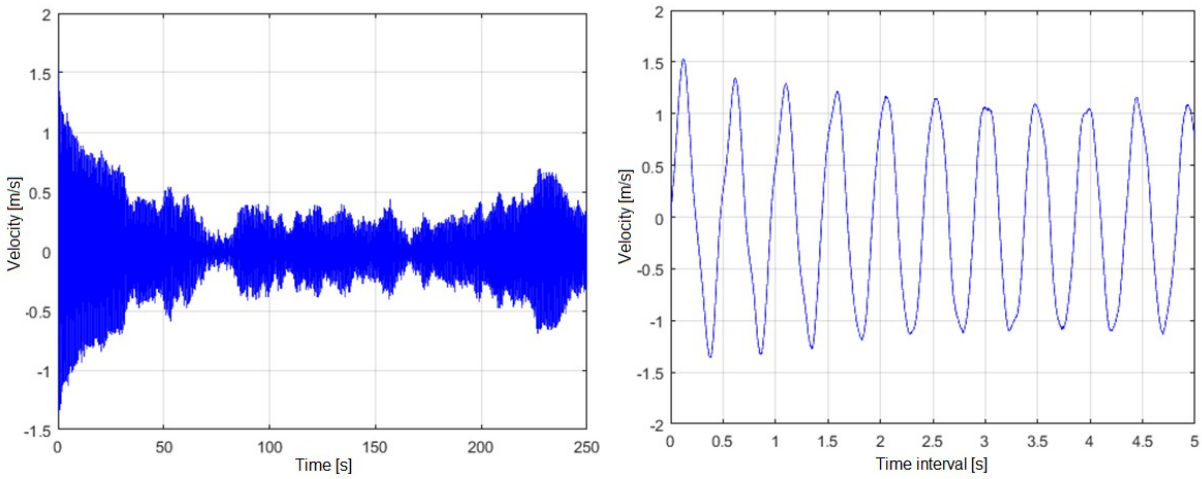

(a) (b)

Figure 9 – Velocity at point A at t = 250 s (a) and zoom in (b).

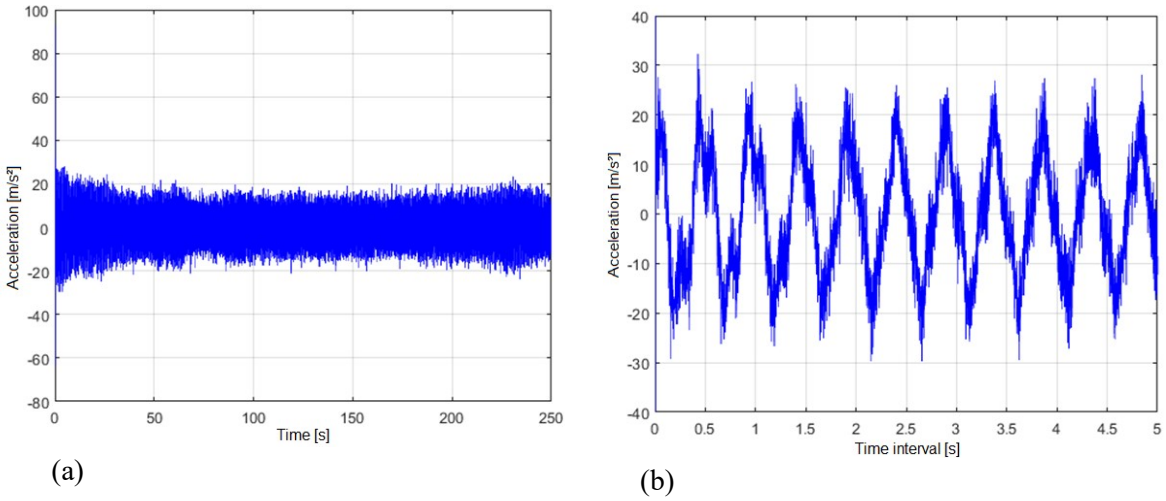

(a) (b)

Figure 10 – Acceleration at point A at t = 250 s (a) and zoom in (b).

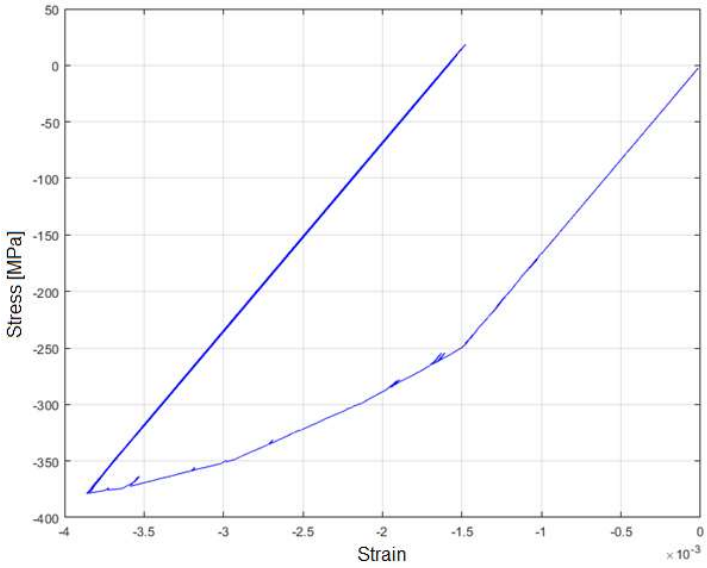

Figure 11 – Plane steel frame stress x strain hysteresis curves.

Also, an error analysis was performed on a refining **h**, where the mesh 1 has 9 elements, the mesh 2 has 18 elements, the mesh 3 has 36 elements and, finally, the mesh 4 has 72 elements.

The Figures 12 and 13 show the refining **h** errors behavior along the first 5 seconds of analysis. For the three results: acceleration, velocity and displacement, it is possible to see the high error for mesh 1 and 2 and a lower for mesh 3 and 4. However, the results of errors for acceleration remain high when compared to the displacement errors. For the acceleration and displacement errors the refining **h** has an improvement of approximately 90% and 37%, respectively.

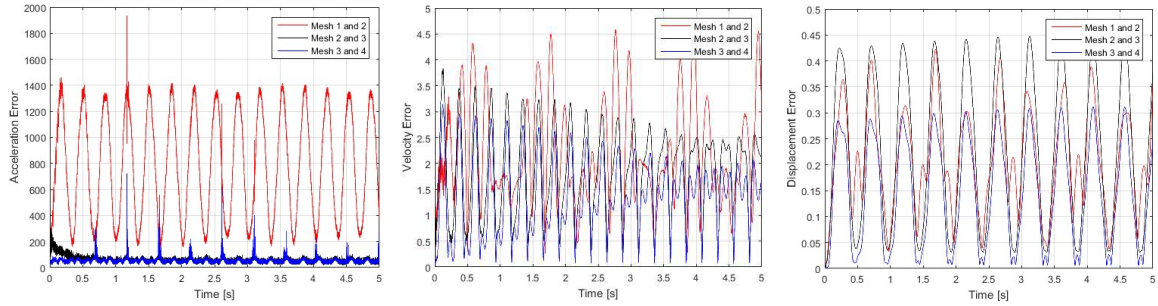

(a) (b) (c)

Figure 12 – Refining h errors for acceleration, velocity and displacement in the first 5 s.

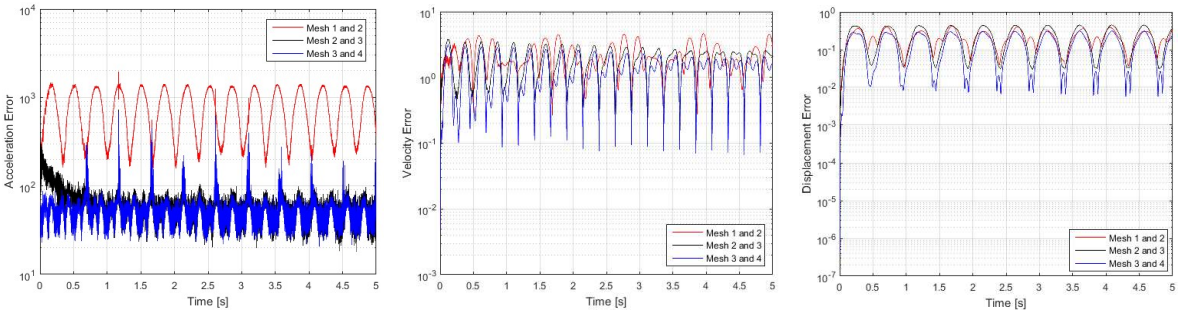

(a) (b) (c)

Figure 13 – Refining h errors for acceleration, velocity and displacement in the first 5 s.

5 Conclusions

The employed methodology for evaluation of random excitation in this work is based on the theory of stochastic modelling of wind action, where the velocity of the wind is determined by the Shinozuka and Jan mode, with different wind spectra. The wind loading profile along the height of the structure and over the time has a random behavior, since the phase angle is determined randomly.

The dynamic elastoplastic behavior of the structure, subject to different wind spectra, is analyzed in the several examples. The hysteresis curve of stress and strain is calculated, as well as the mechanical behavior of the structure, such as displacement, velocity and acceleration, is also obtained from the analyzed structure. The relative difference is also calculated for the displacement of the structure subjected to different wind spectra. These have similar characteristics to the one known in the literature. However, with the input data used in this work, Kaimal and Davenport wind spectrum produces dynamic elastoplastic responses in the structure, with 7% of relative difference approximately. From the observation on wind loading profile, the Davenport and Harris spectra present higher oscillation frequency, while the Kaimal and von Kármán spectra present lower oscillation frequency. However, these characteristics does not affect significantly the structure response. Furthermore, the displacement and velocity responses obtained from von Kármán spectrum have smaller amplitude in the oscillation during the time range covered in this study. This occurs since the von Kármán's wind loading has more uniform action and less amplitude in the oscillation.

Acknowledgment

The author would like to acknowledge the financial support provided by CAPES (Foundation affiliated with the Ministry of Education of Brazil).

References

[1] Armero, F. and Romero, I., Energy-dissipative momentum-conserving time-stepping algorithms for the dynamics of nonlinear cosserat rods, *Computational Mechanics*, 31, 3-26, 2003.

[2] Bathe, K. J, *Finite element procedure,* Prentice-Hall, New Jersey, USA, 1996.

[3] Brazilian association of technical standards NBR-6123, *Forces due to the wind in buildings*, ABNT, Rio de Janeiro, Brasil, 1988.

[4] Balendra, T., *Vibration of buildings to wind and earthquakes loads*, Springer-Verlag, New York, USA, 1993.

[5] Blessmann, J., Buffeting effects on neighbouring tall buildings, *Journal of Wind Engineering and Industrial Aerodynamics*, Amsterdam, 18, 105-110, 1985.

[6] Carassale, L. and Solari, G., Monte Carlo simulation of wind velocity fields on complex structures, *Journal of Wind Engineering and Industrial Aerodynamics*, 94(5), 323–339, 2006.

[7] Chang, S. Y., A new family of explicit methods for linear structural dynamics, *Computers and Structures*, 88, 755-772, 2010.

[8] Chen, W. F. and Sohal, I. *Plastic design and second-order analysis of steel frames,* Springer-Verlag, New York, USA, 1995.

[9] Chopra, A. K., *Dynamics of structures – Theory and Applications to Earthquake Engineering,* Prentice-Hall, New Jersey, USA, 1995.

[10] Chung, J. and Hulbert, G. M., A time integration algorithm for structural dynamics with improved numerical dissipation: the generalized – alfa method, *Journal of Applied Mechanics*, 60, 371-375, 1993.

[11] Davies, J. M., Second-order elastic-plastic analysis of plane frames, *Journal of constructional steel research*, 58, 1315-1330, 2002.

[12] Feng, C. and Chen, X., Inelastic responses of wind-excited tall buildings: Improved estimation and understanding by statistical linearization approaches, *Engineering Structures*, 159, 141-154, 2018.

[13] Ferraro, V., Irwin, P. A. and Stone, G. K., Wind induced building accelerations, *Journal of Wind Engineering and Industrial Aerodynamics*, 36, 757-767, 1990.

[14] Huang, M.; Tu, Z.; Li, Q. and Lou, W., Dynamic wind load combination for a tall building based on copula functions, *International Journal of Structural Stability and Dynamics*, 17(8), 2017.

[15] Garg, N. and Han, C., Axisymmetric couple stress elasticity and its finite element formulation with penalty terms, *Archive of Applied Mechanics*, 85, 587-600, 2014.

[16] Goudreau, G. L. and Taylor, R. L., Evaluation of numerical integration methods in elastodynamics, *Computer Methods in Applied Mechanics and Engineering*, 2, 69-97, 1972.

[17] Gu, M. and Quan, Y., Across-wind loads of typical tall buildings, *Journal of Wind Engineering and Industrial Aerodynamics*, 92(23), 1147-1165, 2004.

[18] Hilber, H. M., Hughes, T. J. R. and Taylor, R. L., Improved numerical dissipation for time integration algorithms in structural dynamics, *Earthquake engineering and structural dynamics*, 5, 283-292, 1977.

[19] Horne, M. R. and Morris, L. J.*, Plastic design of low-rise frame,* Granada Publishing Limited. Great Britain, 1981.

[20] Isyumov, N., Alan G. Davenport's mark on wind engineering, *Journal of Wind Engineering and Industrial Aerodynamics*, 104-106, 12–24, 2012.

[21] Jeyakumar, M. and Christopher, T. Influence of residual stresses on failure pressure of cylindrical pressure vessels, *Chinese Journal of Aeronautics*, 26(6), 1415-1421, 2013.

[22] Kareem, A., Ge, Y. and Zhao, L., Fluctuating wind pressure distribution around full-scale cooling towers, *Journal of Wind Engineering and Industrial Aerodynamics*, 165, 34–45, 2017.

[23] Kim, S.; Kim, Y. and Choi, S., Nonlinear analysis of 3-D steel frames, *Thin-Walled Structures*, 39, 445-461, 2001.

[24] Muscolino, G. and Sofi, A., Response statistics of linear structures with uncertain-but bounded parameters under Gaussian stochastic input, *International Journal of Structural Stability and Dynamics,* 11, 775-804, 2011.

[25] Li, Q. S. et al., Dynamic behavior of Taipei 101 Tower: field measurement and numerical analysis, *Journal of Structural Engineering*, 137(1), 143-155, 2011.

[26] Lin L, Ang, A. H. S., Xia D. D., Hu, H. T., Wang, H. F. & He, F. Q., Fluctuating wind field analysis based on random Fourier spectrum for wind induced response of high-rise structures, *Structural Engineering and Mechanics*, 63(6), 837-846, 2017.

[27] Mohebbi, M., Joghataie, A. and Dabbagh, H., Effect of response related weighting matrices on performance of active control systems for nonlinear frames, *International Journal of Structural Stability and Dynamics*, 17, 1750030, 2017.

[28] Orbison, J. G., Mcguire, W. and Abel, J. F., Yield Surface Applications in Nonlinear Steel Frame Analysis, *Computer Methods in Applied Mechanics and Engineering*, 33, 557-573, 1982.

[29] Rahman, S. Wiener-Hermite polynomial expansion for multivariate Gaussian probability measures, *Journal of Mathematical Analysis and Applications*, 454, 303-334, 2017.

[30] Repetto, M. P. and Solari, G., Dynamic alongwind fatigue of slender vertical structures, *Engineering Structures*, 23, 1622–1633, 2001.

[31] Reis, D. G., Siqueira, G. H., Vieira Junior, L. C. M. and Ziemian, R. D., Simplified approach based on the natural period of vibration for considering second-order effects on reinforced concrete frames, *International Journal of Structural Stability and Dynamics*, 18, 1850074, 2017.

[32] Shang, H. Y., Machado, R. D. and Abdalla Filho, J. E., Dynamic analysis of Euler-Bernoulli beam problems using the Generalized Finite Element Method, *Computers and Structures*, 173, 109-122, 2016.

[33] Shang, H. Y., Machado, R. D., Abdalla Filho, J. E. and Arndt, M., Numerical analysis of plane stress free vibration in severely distorted mesh by Generalized Finite Element Method, *European Journal of Mechanics A/Solids*, 62, 50-66, 2017.

[34] Shinozuka, M. and Jam, C. M., Digital simulation of random process and its Applications, *Journal of Sound and Vibration*, 25(1), 111-118, 1972.

[35] Wang, H., Guo, T., Tao, T. and Li, A., Study on wind characteristics of Runyang suspension bridge based on long-term monitored data, *International Journal of Structural Stability and Dynamics*, 2016.

[36] Wang, Y., Hu, Q., Meng, D. and Zhu, P., Deterministic and probabilistic wind power forecasting using a variational Bayesian-based adaptive robust multi-kernel regression model, *Applied Energy*, 208, 1097-1112, 2017.

[37] Zhang, L. L., Li, J. and Peng, Y., Dynamic response and reliability analysis of tall buildings subject to wind loading, *Journal of Wind Engineering and Industrial Aerodynamics*, 96, 25–40, 2008.

[38] Zhi, L. H., Chen, B. and Fang, M. X., Wind load estimation of super-tall buildings based on response data, *Structure Engineering and Mechanics*, 56, 625-648, 2015.

[39] Zhi, L. H., Pan, Y., Tu, J., Bo, C. and Li. Y., A Kalman filter based algorithm for wind load estimation on high-rise buildings, *Structure Engineering and Mechanics,* 64(4), 449-459, 2017.

[40] Zhou, Z. and Murray, D. W., Pipeline beam models using stiffness property deformation relations, *Journal of Transportation Engineering*, 122(2), 164 – 172, 1996.